Performance Evaluation of Microfiltration and Centrifugation for Separating Suspended Solids from Fermented Molasses Solution

Faraji, Foad; Mehranbod, Nasir*+

School of Chemical and Petroleum Engineering, Shiraz University, Shiraz, I.R. IRAN

Sarshar, Mohammad

Institutes of Mechanics, Shiraz, I.R. IRAN

ABSTRACT: *Ethanol is considered a renewable fuel that can be produced via fermentation of sugarcane molasses. The fermented solution that is fed to the distillation column has suspended solid content that tends to block distillation trays leading to low ethanol recovery. In this study, performances of microfiltration and centrifugation processes were investigated for the separation of suspended solids from the fermented solution of sugarcane molasses. The filtration process using a ceramic filter under pressure differences of 1, 2, 3, and 4 bars was studied. Based on the results of this study, the overall filtration process can be divided into three stages pore blocking, cake filtration, and cake layer compression which were more pronounced as pressure difference across filter media increased. In addition, increasing pressure difference across the filter caused a sharp decrease in permeate flux due to faster pore blocking and higher turbidity removal, 96.99% due to cake filtration, and compaction of the cake layer. A comparison of curve-fitted experimental data and blocking models showed that the full cake model had the best fit with an Average Absolute Relative Error (AARE) of 0.112. Further, in this study, experimental design was used to optimize the operating parameters of centrifugation for separation and removal of suspended solids from fermented solution. Single complete and complete-standard models among blocking models had the best fit for filtration after centrifugation under optimal operating conditions that correspond to the filtration pressure difference of 4 bars. The measured data showed that the permeate volume in centrifugation plus filtration increased about threefold compared to filtration alone, although the turbidity removal decreased slightly from 96.99 to 89.78%.*

KEYWORDS: *Suspended solids; Ethanol Fermentation; Microfiltration; Blocking Models; Centrifugal separation.*

INTRODUCTION

Most of the energy consumption worldwide is based on burning fossil fuels that adversely affect the environment and such fuels themselves are non-renewable [1]. Moreover, industrial development and population growth

* *To whom correspondence should be addressed.*
+ E-mail: mehran@shirazu.ac.ir
1021-9986/2023/11/3917-3928 12/$/6.02

have made the ever-increasing fossil fuel consumption a global problem [2]. This has challenged scientists to reduce fossil fuel reserves and emission of greenhouse gases by finding alternative energy resources that are renewable, sustainable, low cost, safe, and efficient [3]. Replacement of fossil fuels with renewable energy sources such as solar, biomass, wind, and hydroelectricity energies has been studied in recent years. In the meantime, biomass sources due to their high potential in the production of solid, liquid, and gas fuels have received widespread attention [4]. The developed means of conversion of biomass into biofuels illustrates the importance of exploiting a renewable energy source for reducing pollutant emissions, especially carbon dioxide.

One of the most important liquid biofuels is ethanol which is used as a renewable fuel and as a substitute for Methyl Tertiary-Butyl Ether in gasoline or as an oxygen carrier in diesel fuel [5]. There are two methods to produce ethanol, biological processes and chemical processes. In the production of ethanol in the biological process, ethanol is produced from three groups of substrates that are sugary foods, starch, and cellulose. Nowadays, 98% of the ethanol produced in the world is obtained by sugar fermentation, which can be conducted by fermenting sugar of many raw materials such as sugarcane and sugar beet molasses [6,7]. Molasses is a sugar mill by-product that is typically used as an additive to animal feed and to produce biofuel via fermentation. Molasses is currently one of the cheapest sources of sugar. Unlike corn and cereal grains, it does not require starch hydrolysis for sugar production prior to fermentation [8,9]. The formation of sticky and very hard to remove fouling on the active area of distillation tower trays is one of the most challenging issues that distillation units of ethanol factories utilizing sugarcane molasses face. [10]. Separation of suspended solids from sugarcane molasses fermented solution can be performed via liquid solid separation methods such as filtration, flotation, coagulation, flocculation and settling.

In this study, due to selectivity of the separation, lower operating costs and better output quality, filtration process is investigated. Filtration separation is carried out by passing a mixture of liquid and solid through a filter media that retains solid particles and causes discharge of suspended particle-free liquid [11]. In filtration process, all the fluid can be passed through filter media pores and the suspended particles with a size larger than the diameter of the filter media pores are retained [12]. However, their use in industrial applications is constrained by their propensity to suffer from severe filter media pore fouling that reduces permeate flux which has been investigated by different blocking models and mechanisms [13].

Hermans and *Bredre* studied the filtration and fouling mechanisms of pore fouling. *Gonsalves et al*. and *Grace* studied physical models to identify the phenomenon of fouling and analysis of blocking models and their relationship to filter media performance [14,15]. *Shirato et al*. developed pore-blocking models for non-Newtonian fluids [16]. Hermia, in 1982, introduced a new version of fouling mechanisms, which became a suitable model for demonstrating mechanisms of fouling. These mechanisms were divided into four main models based on the interaction mechanism between the particles and the filtration media which are intermediate blocking, complete blocking, cake formation, and standard blocking [17].

In the complete model, it is assumed that the entering particles remain close to the pores causing the liquid flow to decrease. In the intermediate blocking model, it is assumed that particles, the same as in the complete model, remain close to the pores or are placed on the other particles on the filter media surface. In the standard blocking model, it is assumed that the particles are located inside the pores and stick to the pore wall that causes the pores free area to decrease. In the cake formation model, several layers of the particles completely cover the filter media surface. Hence, cake layers thickness is increased while filtration is carried out [18].

Bowen et al. observed that Bovine Serum Albumin (BSA) blocked pores in membranes and stirring the system had no effect on reducing flux, and the best model for predicting fouling was the standard model [19]. *Bolton et al*. in addition to examining single blocking models introduced new combined blocking models in both constant pressure and constant flow operating modes. They also examined blocking mechanisms for BSA and human plasma Immunoglobulin G. The combined Cake-Intermediate model was the dominant blocking model for BSA and the Cake-Complete combined model was the dominant blocking mechanism for Immunoglobulin G. [18]. *Kumar et al*. investigated the constant pressure dead-end filtration process for a mixture of Saccharomyces cerevisiae in distilled water using alumina ceramic membrane. They examined the blocking mechanisms

according to Hermia's models and tested cake formation and cake resistance under various operating conditions such as different concentrations of yeast, membrane pore size and several different pressure differences across membrane. As expected, the experimental data showed that flux increased with increasing pore size and also decreased with increasing yeast concentration. In addition, the specific resistance of the cake increased as pressure difference across membrane increased. They showed that the cake blocking mechanism was more dominant than other mechanisms [20]. *Muthukumar et al*. investigated the purification and clarification of fermentation broth for separation of Pichia pastoris, which was a yeast species used in the production of a protein for protein therapy. They investigated microfiltration, filtration using deep filters and separation with centrifuge. The experimental measurements did not fit well with any of the single models; thus, it was concluded that more than one mechanism was involved in pores blocking. Data on deep filters with small pores fitted the cake-complete model and data obtained on deep filters with large pores fitted the cake-intermediate model [21]. *Zhenzhou et al*. investigated the dead-end filtration of sugar beet syrup, which was associated with impurities such as protein and pectin. Such impurities were involved in syrup due to concentrating process in sugar mill at 75 °C and caused problems in downstream operations. They investigated the mechanisms of blocking pores in both unstirred and stirred syrup using Polyethersulfone (PES) and Regenerated Cellulose (RC) membranes. In unstirred state, due to the deposition of particles over the membrane surface, the flux was decreased rapidly. The best model for unstirred condition was complete-cake blocking for the PES membrane and the cake model for the RC membrane. In the stirred state, particle deposition on membrane surface was delayed and the complete blocking model had the best fit for both membranes. Experimental data revealed that the RC membrane is capable of providing higher flux while PES membrane showed better rejection performance [22]. *Kovaleva et al*. evaluated the separation of mature molasses broth, using a microfiltration system with MMPA+, MPS, and MFFK membranes. MMPA+, MPS, and MFFK are basically hydrophilic polyamide, hydrophilic polyethersulfone and fluoroplastic-based membranes. During the filtration of the solution, a dynamic membrane formed, serving as a 100% barrier to yeast biomass and passing more than 80% of ethyl alcohol. They showed for MFFK and MPS membranes, flux increased as the trans-membrane pressure increased. However, MMPA+ membranes' performance is affected by rapid pore blocking and adsorption [23]. *Mubashir et al*. separated suspension of sludge under dynamic mode filtration to evaluate the blocking mechanisms that caused flux reduction. They carried out experiments using gravity driven filtration under various operating conditions. Experimental data revealed that flux was decreased with increasing the concentration and the pore size did not have considerable effects on the flux. They concluded that the effective blocking model was cake filtration mechanism that caused the flux reduction [24]. *Shi et al*. investigated the effects of pretreatment on sugarcane juice and juice composition, using a ceramic membrane with a pore size of 20 nm. Pretreatment of sugar can juice by heating and sedimenting at defined pHs was evaluated, using evaporator supply juice. They observed boiled juice, contained higher proportions of microcrystalline and crystalline phases, and other impurities that reduced membrane filtration efficiency as the cake resistance. The results showed that combined cake -complete blocking was dominate fouling mechanism for partially clarified juice [25]. *Ghalami Choobar et al*. investigated a cross-flow microfiltration system, using mixed cellulose ester membrane for laundry wastewater treatment. The accuracy of curve fitting of experimental data and used models was evaluated by regression coefficient (R^2) and Root Mean Square Error (RMSE). The results showed that the Cake formation model in single stage models was the dominant blocking model with R^2 greater than 0.94 for flux decline. In addition, they investigated more details which showed a three-stage model including a complete model in first stage, an intermediate model in second stage and a cake formation model in last stage with significant accuracy ($R^2 > 0.96$) could predict flux decline. The results also showed an increase in the operation pressure causes the system to be affected more significantly by cake formation model while increasing feed flow rate revealed opposite behavior [26]. *Sjölin et al*. investigated purification of molasses that contains large amounts of sucrose, using ceramic tubular ultrafiltration and nanofiltration membrane. They showed, high filtration fluxes can be obtained and sucrose can be separated from other compounds, but the separation efficiency was generally higher with diluted molasses

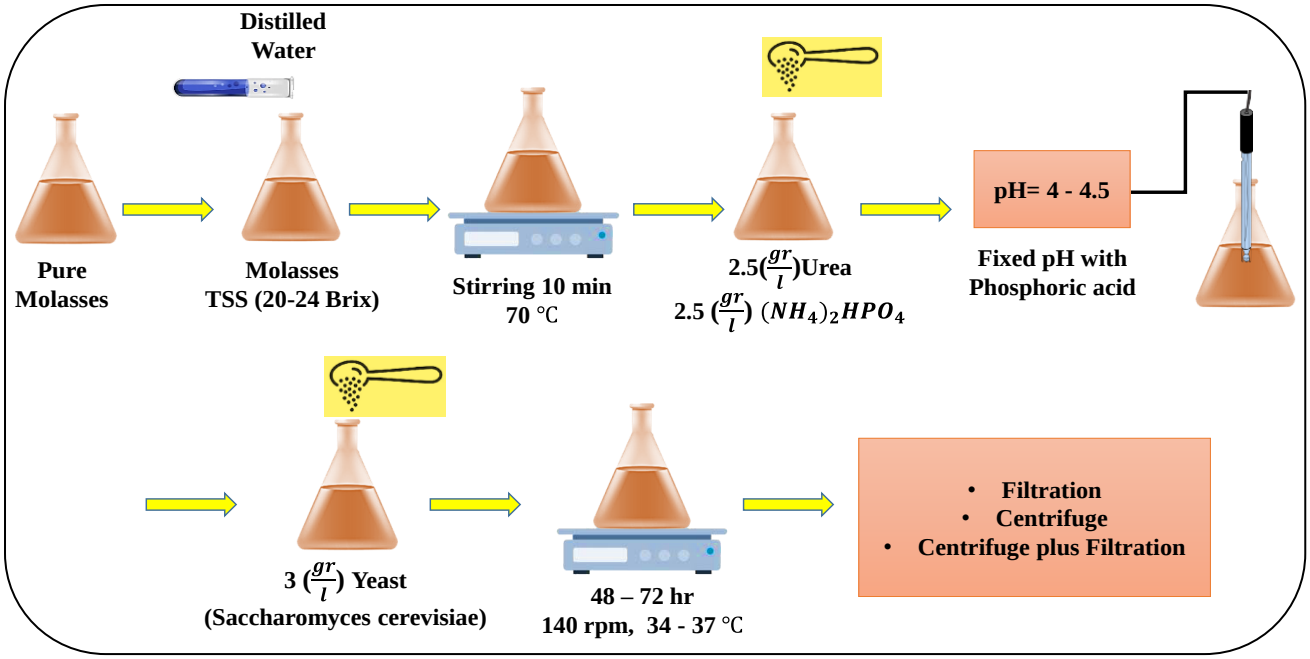

Fig. 1: Flowchart of fermentation process

compared with concentrated molasses. The results revealed more severe fouling when filtering dilute molasses that is potentially due to aggregate formations in molasses [9].

To the best of the authors' knowledge, no study has been published in the open literature on the separation of yeast from fermented molasses solution by microfiltration and combined centrifuge and microfiltration. The yeast in fermented broth for ethanol production tends to cause a malfunction in downstream process equipment. In this work separation of yeast from fermented broth for ethanol production was studied. As such, the production of ethanol from molasses was performed based on the fermentation process in the presence of Saccharomyces cerevisiae. Dead-end microfiltration using a ceramic filter was applied and flux reduction modeling was investigated by Bolton equations that are presented in Table 1 [18]. Filtration under four pressure differences across filter media was applied to investigate the mechanisms of blocking models. Further, centrifugal separation and combined filtration and centrifugal separation were also investigated.

EXPERIMENTAL SECTION

Materials

Molasses was supplied from a local sugarcane mill and the yeast (Saccharomyces cerevisiae) was purchased from Razavi Company. Urea, ammonium dihydrogen phosphate and phosphoric acid were purchased from Merck Company. Ultracarb ceramic filter media with 65.3% porosity and average pore size of 0.45 µm was made from Kieselguhr and was purchased from Royal Doulton Company. The filter media was cylindrical with an outer diameter of 45 mm and a thickness of 8 mm with the length of 25 mm providing 0.003535 m^2 filtering surface area.

Fermentation

The fermentation method used in this study is as practiced in Haft Tappeh Sugarcane Agro-Industry Co. and is presented pictorially in Fig. 1. In this method, 170 g (130 mL) of 80 Bx molasses is diluted with distilled water with a dilution factor of 5 to achieve total soluble solids of 20 Brix. Total soluble sugar is measured using refractometer Huixia SBR-32T. The mixture is kept at 70 °C for 10 min for pasteurization. Then, 2.5 g/l of urea and 2.5 g/L of ammonium dihydrogen phosphate are added and pH is adjusted to 4- 4.5 using phosphoric acid. 3 g/L of yeast (Saccharomyces cerevisiae) is added and is stirred at 140 rpm and temperature of 34-37 °C for 48 to 72 h. until completion of the fermentation process.

Filtration

The filtration set-up is shown schematically in Fig. 2 consists of a N_2 gas cylinder that is connected to a 500 mL vessel connected to a filtration module and equipped with a pressure gauge. The ceramic membrane can be

Table 1: Different mathematical filtration model for single (classic) and combined models [18]

Single Models		
Standard	$V = \left(\frac{1}{tJ_0} + \frac{K_s}{2}\right)^{-1}$	$K_s(1/m)$
Intermediate	$V = \frac{1}{K_i}\ln(1 + K_i J_0 t)$	$K_i(1/m)$
Complete	$V = \frac{J_0}{K_b}\left(1 - \exp(-K_b t)\right)$	$K_b(1/s)$
Cake	$V = \frac{1}{K_c J_0}\left(\sqrt{1 + 2K_c {J_0}^2 t} - 1\right)$	$K_c(s/m^2)$
Combined Models		
Cake – Complete	$V = \frac{J_0}{K_b}\left(1 - \exp\left(\frac{-K_b}{K_c {J_0}^2}\left(\sqrt{1 + 2K_c {J_0}^2 t} - 1\right)\right)\right)$	$K_b(1/s)$, $K_c(s/m^2)$
Cake – Intermediate	$V = \frac{1}{K_i}\ln\left(1 + \frac{K_i}{K_c J_0}\left(\left(1 + 2K_c {J_0}^2 t\right)^{0.5} - 1\right)\right)$	$K_c(s/m^2)$, $K_i(1/m)$
Complete – Standard	$V = \frac{J_0}{K_b}\left(1 - \exp\left(\frac{-2K_b t}{2 + K_s {J_0}^2 t}\right)\right)$	$K_b(1/s)$, $K_s(1/m)$
Intermediate – Standard	$V = \frac{1}{K_i}\ln\left(1 + \frac{2K_i J_0 t}{2 + K_s J_0 t}\right)$	$K_s(1/m)$, $K_i(1/m)$

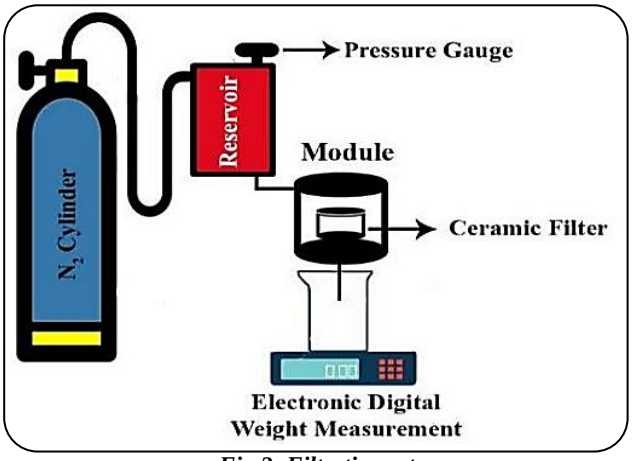

Fig 2: Filtration set-up

placed in the sealed filtration module is of 2.5 cm in height and has an effective surface area of 35.35×10^{-4} m^2. The filtration is carried out at four pressure differences of 1, 2, 3, and 4 bars across filter media. The weight of the filtrated solution is measured during a filtration run and using solution density the cumulative curve of filtrate volume as a function of time can be plotted that constitutes a data set.

Single and combined Bolton models that are shown in Tables 1 are used to determine the best model that can fit experimental data. Any experimental data set is randomly divided into train and test data that consists of 72% and 28% of data in a data set. All models of Table 1 were examined using ta to minimize Sum of Squared Residual (SSR) to determine the best value for the blocking model parameter/parameters.

SSR is the sum of difference between the experimental and predicted data that can be calculated using Eq. (1). Then, Average Absolute Relative Error (AARE) based on Eq. (2) is calculated for training data for all fitted models to determine the model that can best describe experimental data set.

$$SSR = \sum\left(Y_{exp} - Y_m\right)^2 \quad (1)$$

$$AARE = \left(\sum\left(\frac{|Y_{exp} - Y_m|}{Y_{exp}}\right)\right)/n \quad (2)$$

Centrifugal separation

Centrifugation tests were carried out under different operation conditions that include centrifugation times of 1, 2, 3, 4, 5, and 6 minutes and centrifuge speeds of 500, 1000, 1500, 2000, 2500, and 3000 rpm. Net energy consumption (kJ) and turbidity of product solution (NTU) for each test are measured and used as the objective response. Hence, thirty-six experiments were identified according to the general factorial method and the results were analyzed using Design Expert software. A watt-meter (DW-6060) is connected to the centrifuge separator (Eppendorf 5810 R) to measure the consumption power as a function of time and speed. During the separation, the measured power of the device is converted to energy. The turbidity of the solution is measured using the turbidity meter (HACH 2100 P). Based on the experimental data, the optimal point is determined at minimum energy and turbidity.

Table 2: Carbohydrates' concentration in fermentation broth and fermented solution

Carbohydrates	Concentration (mg/L)	
	Diluted molasses	Fermented broth
Sucrose	373.18	319.29
Glucose	1147.23	276.01
Fructose	94.27	57.55

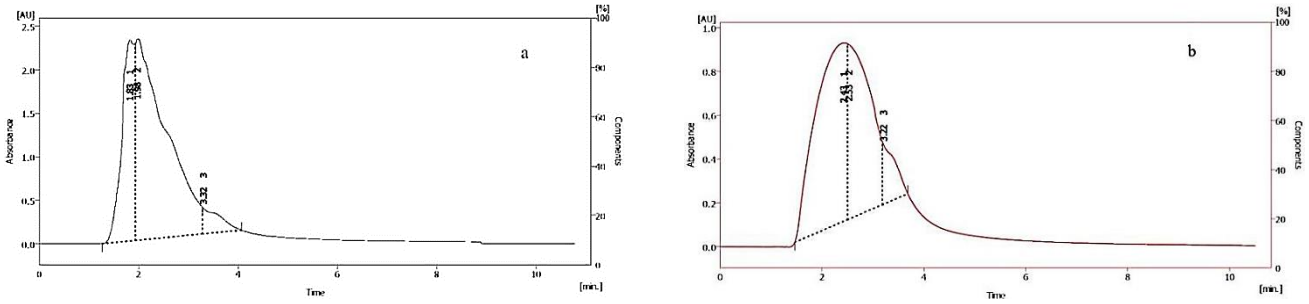

Fig. 3: HPLC chromatogram for (a) in pure molasses before fermentation (b) fermented solution

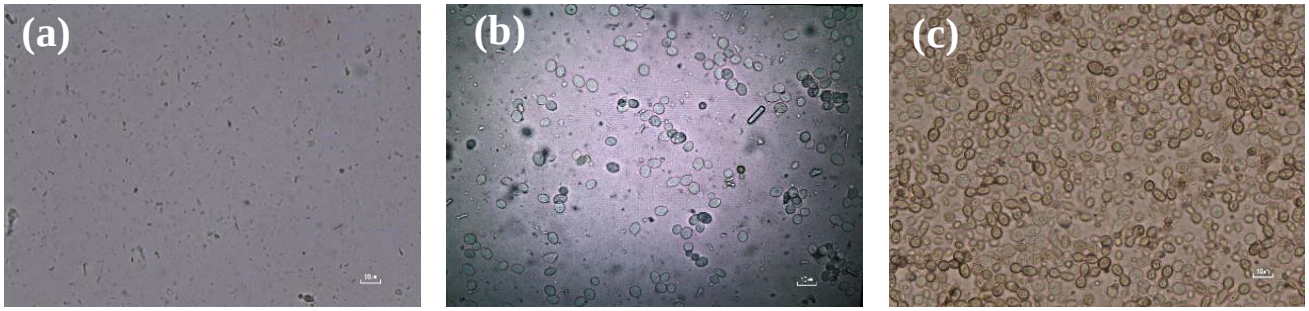

Fig 4: Microscopic images (40X magnification), (a) diluted molasses, (b) molasses after adding yeast, (c) molasses after the fermentation process

RESULTS AND DISCUSSION

High-Performance Liquid Chromatography (HPLC) analysis is used to confirm sugar concentration through the fermentation process. Three peaks of HPLC measurements represent the carbohydrates in the solution such as sucrose, glucose and fructose, are shown in Figs. 3(a) and (b) for molasses and fermented solutions, respectively. According to the peak areas, concentrations of sucrose, glucose, and fructose at diluted molasses and fermented broth are shown in Table 2. The carbohydrate concentrations indicate that the dominant carbohydrate in the molasses is Glucose and it is mostly consumed in the fermentation process.

Images of suspended solids in the molasses solution through the fermentation process are prepared via microscope (Nikon ECLIPSE E200), using 40X magnification. An image of diluted molasses in Fig. 4(a) shows that the suspended solids in the diluted molasses solution are negligible and originate from a sugarcane mill operation. Suspended solid image after the addition of yeast to the solution is shown in Fig. 4(b). It reveals the presence of a limited number of yeast particles that are dispersed in the solution. A microscopic image of the molasses solution after completing the fermentation process is shown in Fig. 4(c). It clearly shows that numerous numbers of yeast cells indicate the growth of the yeast through the fermentation process. Such suspended solids are troublesome once settled on the trays of the distillation tower during ethanol purification.

Particle size distribution is measured using microscopic images and image processing software. Particle size distribution for the fermented solution is shown in Fig. 5 that indicates most of the particles have diameters in the range of 4-7 μm.

Modified measured filtration rate profiles are shown in Figs. 6 and 7 for 1 bar and 2 to 4 bars, respectively. In the modified profile the ratio of filtration time to filtrate volume is plotted versus total filtrate volume at a given time. As shown in the figures, the filtration process is divided into different stages, which is consistent with

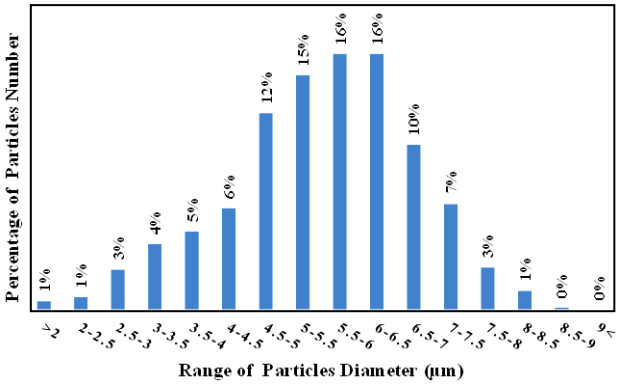

Fig. 5: Differential particle size analysis of fermented solution

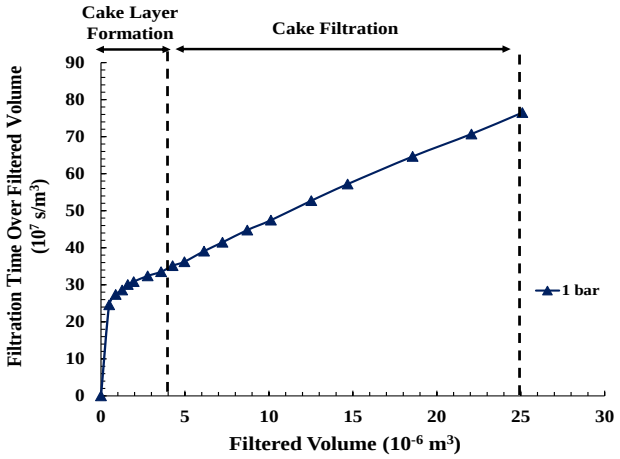

Fig. 6: The ratio of filtration time to filtrate volume as a function of the total volume filtered at 1 bar

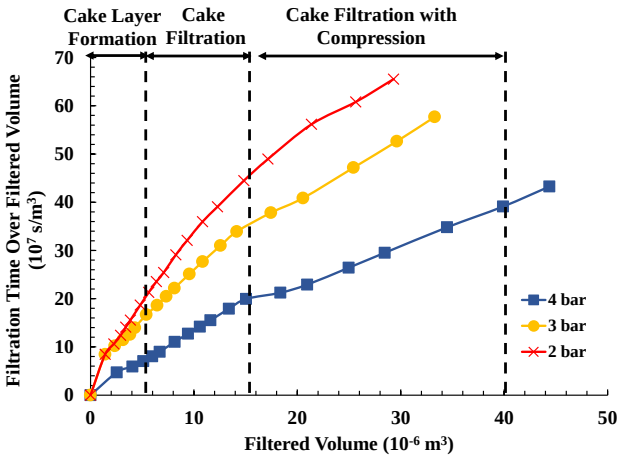

Fig. 7: The ratio of filtration time to filtrate volume as a function of the total volume filtered at 2, 3 and 4 bar

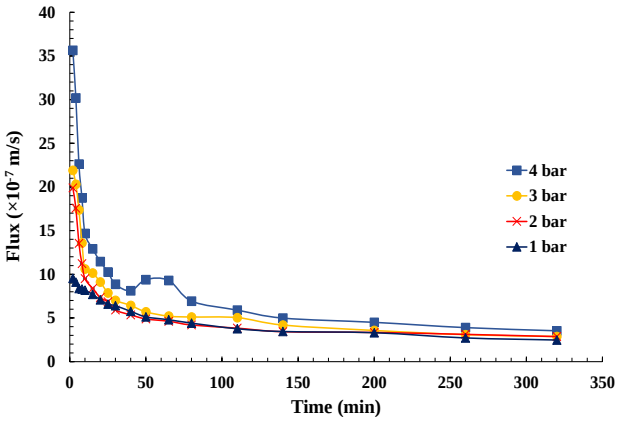

Fig. 8: Flux decline with time at different pressures

studies of *Schippers et al*. [27]. In the first stage, the pores are blocked with particles and the cake layer is gradually formed. In the second stage, the cake filtration takes place and in the last stage, the cake layers are compressed.

The formation of cake layers occurs by pore blocking in the first stage and cake filtration starts in the second stage. Normally, in the third stage, compression of cake layer formed in the two previous stages starts. However, compression of cake layers requires enough pressure difference across cake and may not happen in all cases. An example is the data presented in Fig. 6 for the pressure difference of one bar that was not high enough to cause cake compression.

The filtration profile as shown in Fig. 7 indicates that the cake layer is formed initially and then is gradually changed to cake filtration with the slow retention of smaller particles and the cake layers are compressed and thickened with time in the third stage. The particles are deformed in the third stage by the pressure and the compressed cake layers cause the filtrate rate to decrease while enhancing filtrate clarity.

As the filtrate flux profile shown in Fig. 8, a sharp decrease of filtrate flux is experienced first in filtration process followed by a region in which flux decreases very slowly. This is due to pore blockage during the first stage of filtration and cake filtration and compression in the second and third stages of filtration. The flux changes under one bar pressure difference shown in Fig 8. does not experience a sudden change in flux that can be attributed to the gradual particle accumulation on filter surface and slow formation of cake layers.

The experimental data and the model predictions based on single and combined models at 4 bars are shown in Figs. 9 and 10, respectively. As can be observed from these two figures the cake and cake-complete models seem to fit data much better than other models. AARE calculated for training data, test data, and the sum of these two for all single and combined models are also presented in Table 3. Based on calculated AARE, the best fit to the experimental data

Table 3: AARE and model parameters for selected blocking models for filtration of fermented solution

Models	ARRE for different sets of data			Fit parameter values
	Training	Test	Total	
Cake-Complete	0.1188	0.0948	0.1120	K_c= 1.54×10^8 (s/m^2), K_b= 6.25×10^{-5} (1/s)
Standard	0.2125	0.1750	0.2021	K_s= 157.89 (1/m)
Complete	0.2763	0.2436	0.2672	K_b= 3.7×10^{-4} (1/s)
Intermediate	0.1579	0.1138	0.1456	K_i= 251.1 (1/m)
Cake	0.1298	0.1152	0.1257	K_c= 1.91×10^8 (s/m^2)

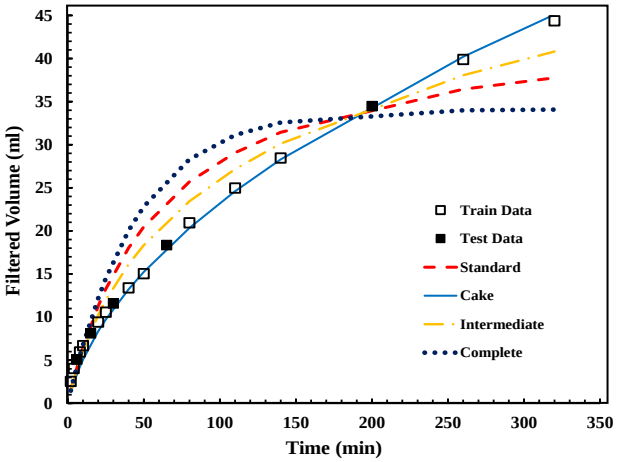

Fig. 9: Experimental data on filtration of fermented solution and single model predictions at 4 bar

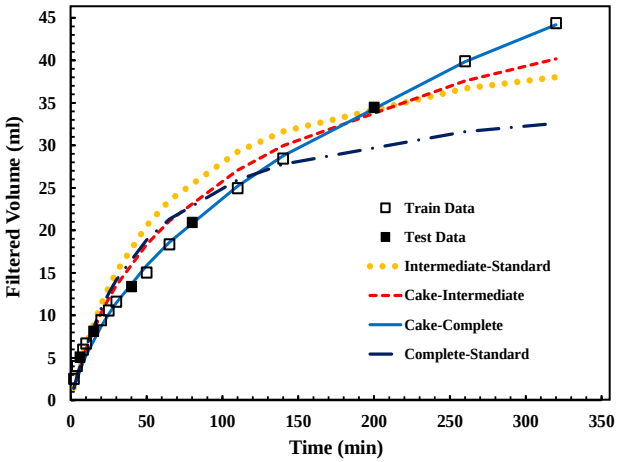

Fig 10: Experimental data on filtration of fermented solution and combined model predictions at 4 bar

is observed to be the cake-complete model with the lowest AARE. However, the cake model alone also fits the experimental data as well as the cake-complete model. The ratio of $(K_c J_0)/(K_b/J_0)$ is 31.22 for a cake-complete model which indicates that the cake model is dominant in comparison with the complete model [18]. Experimental data for other pressure differences of 1, 2, and 3 bar also pointed to the cake model as the prevailing model that can precisely describe the filtration process of fermented molasses solution over the ceramic filter used in this study.

The filtration process can separate almost all of the particles in the fermented solution showing high efficiency in suspended solid rejection and separation. The measured percentages of turbidity removal in the filtrate are 88.71%, 91.18%, 93.44% and 96.99% at four pressure differences of 1, 2, 3 and 4 bars, respectively. Turbidity removal s increased as pressure difference across ceramic filter increased which is due to faster cake layer formation and more cake compression during the filtration process. More cake compaction causes less cake porosity and channels with smaller diameters for the solution to go through. Thus, smaller suspended solids can be retained in the cake leading to higher turbidity removal.

As mentioned, centrifugation was applied to the fermented solution under different speeds and durations. After each centrifuge test, net energy consumption and turbidity of the product solution are measured and used as a response for each test. The full factorial matrix of different operating conditions that include centrifuge speed, ω, and centrifuge duration, t_c, and the responses are analyzed using Design Expert software. For the sake of brevity, a few important ANOVA results from the software are presented in Table 4.

The P-values for variables that significantly affect responses must be smaller than 0.05. Only the variables or combinations of variables that meet the requirement of being significant are included in Table 4. As expected, only these variables or a combination of variables can be included in the correlative equations presented in Table 5. These equations allow accurate prediction of responses given the speed and duration of centrifugation. The numerical values reported in Table 4 for R-squared, Adjusted R-Squared, and Predicted R-squared describe agreement between experimental and predicted data, the effectiveness of model parameters, and the ability of the developed model to predict new data, respectively. The results in Table 4 show the accuracy

Table 4: ANOVA result for centrifugation tests

Model	Source	P-value	Fitting parameter	
Turbidity	t_c - Time (min)	<0.0001	R-Squared	0.9814
	ω - Speed (rpm)			
	ω t_c		Adj R-Squared	0.9776
	ω^2			
	$t_c\omega^2$		Pred R-squared	0.9689
	ω^3			
Energy	t_c - Time (min)	<0.0001	R-Squared	0.9994
	ω - Speed (rpm)			
	ω t_c		Adj R-Squared	0.9993
	ω^2			
	$t_c\omega^2$		Pred R-squared	0.9991
	ω^3			

Table 5: Correlative equations for energy consumption and turbidity of product solution

Energy	$-5217.01 + 5359.45(t_c) + 13.61(\omega) - 3.48(t_c\omega) - 9.15\times10^{-3}(\omega)^2 + 2.31\times10^{-3}(t_c\omega^2) + 1.78\times10^{-6}(\omega)^3$
Turbidity	$849.13 - 49.45(t_c) - 0.785(\omega) + 0.036(t_c\omega) + 3.09\times10^{-4}(\omega)^2 - 7.7\times10^{-6}(t_c\omega^2) - 4.15\times10^{-8}(\omega)^3$

of the proposed models for predicting energy consumption and turbidity are acceptable.

The five different sets of centrifuge speed and duration that are presented in Table 6 are not utilized either in model training and test and are used here for model validation. Centrifuge net energy consumption and turbidity of product solution for these five sets are measured and compared with correlative model predictions. The relative errors are calculated and are reported in Table 6. The experimental and predicted data for energy consumption and turbidity are shown in Figs. 11 and 12, respectively. Based on the calculated relative errors in Table 6 and presented data of Figs. 11 and 12, one can conclude that the correlative models are accurate enough to be used for process optimization.

Optimal values of rotational speed and time centrifugal separation are obtained based on the developed correlative models and the results are shown in Table 7 with model predictions for energy consumption and turbidity. The optimum operation conditions are validated by repeating such conditions three times and the experimental results are presented in Table 8. Accordingly, the relative error for turbidities and energy consumption is very low and as a result, the validity of the optimal point is confirmed.

Table 6: Relative errors (%) between predicted and experimental data for energy and turbidity

ω -Speed (rpm) & t_c –Time (min)	Relative Error (%)	
	Energy	Turbidity
760 (rpm) – 6 (min)	2	6
1140 (rpm) – 8 (min)	4	6
1630 (rpm) – 7 (min)	1	5
2250 (rpm) – 5 (min)	2	5
2770 (rpm) – 4 (min)	2	3

Table 7: Optimum operating conditions for centrifugation process

t_c -Time (min)	Speed (rpm)	Turbidity (NTU)	Energy (kJ)	Desirability
3	1920	160.73	21.43	0.858

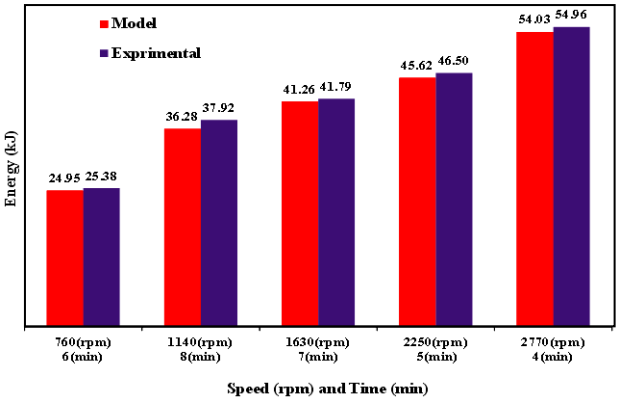

Fig. 11: Experimental and predicted centrifuge energy consumption

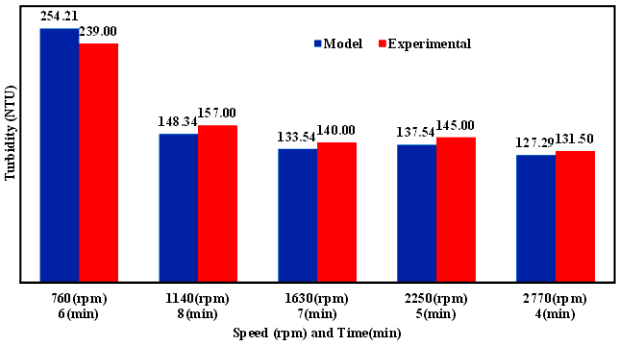

Fig. 12: Experimental and predicted product solution turbidity

To maximize filtrate flux with minimum turbidity, a combination of centrifuge and filtration is also studied. Optimum operating conditions of 1920 rpm and 3 min for a centrifuge are applied to the fermented solution and the product solution is then filtered at 4 bar pressure difference across the ceramic filter. Filtrate volume profile data are used for SSR minimization, blocking model parameter estimation, and model validation that are performed

Table 8: Results of validation tests of the optimum operating conditions

	Experimental data	Model prediction	Average	Standard Deviation	Relative Error (%)
Turbidity (NTU)	167.00 178.00 176.00	160.73	176.3	4.78	7
Energy (kJ)	21.78 22.12 21.90	21.43	21.96	0.14	2

Table 9: AARE and model parameters for selected blocking models for centrifuged solution

Models	ARRE for different sets of data			Fitted parameters
	Training	Test	Total	
Complete-Standard	0.0952	0.0757	0.0890	K_b= 1.14×10^{-2} (1/s) , K_s= 2.8×10^{-3} (1/m)
Standard	0.1064	0.0975	0.1039	K_s= 43.92 (1/m)
Complete	0.0871	0.0765	0.0841	K_b= 1.14×10^{-2} (1/s)
Intermediate	0.2318	0.2439	0.2352	K_i= 122.9 (1/s)
Cake	0.5438	0.5539	0.5497	K_c= 6.96×10^{6} (s/m^2)

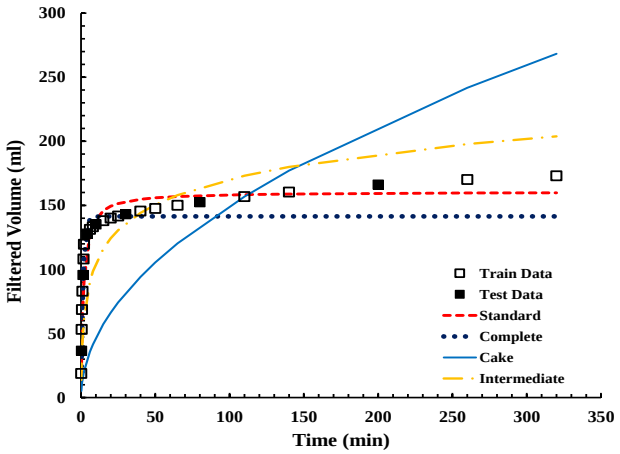

Fig. 13: Experimental data on filtration of centrifuged solution and single model predictions at 4 bar

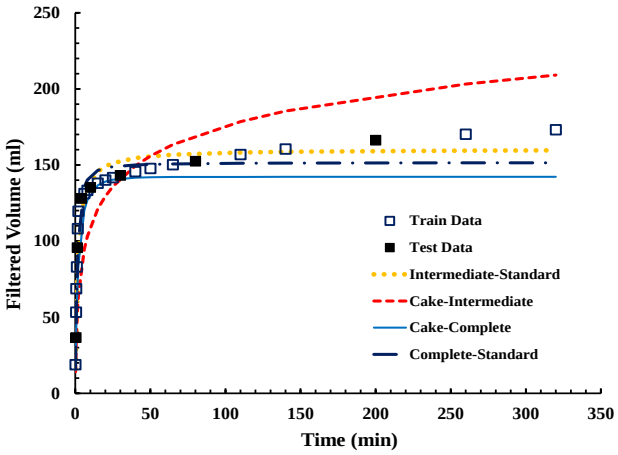

Fig. 14: Experimental data on filtration of centrifuged solution and combined model predictions at 4 bar

for all single and combined models of Table 1. Experimental data and model predictions are presented in Figs 13 and 14 for filtration of product solution from centrifugation. Filtrate volume profiles for filtration of product solution from centrifugation show a very sharp increase in cumulative filtrate volume over a period of around 40 minutes. Then, filtration continues with a very low slope that contributes negligibly to filtrate volume. This is considerably different from filtrate volume profiles presented in Figs. 9 and 10 for filtration alone in which filtration even continued after 350 minutes of operation maintain almost constant slope. Such differences in filtrate volume profiles can be attributed to the separation of large-size suspended solids during centrifugation. The remaining small size suspended solids fed to filtration that are low in concentration thus higher filtrate rates are achievable. However, it seems that such small particles tend to block filter pores permanently leading to a low rate of filtrate volume increase after 40 minutes.

AARE data for filtration of product solution of centrifuge are presented in Table 9 for selected blocking models. It can be observed that combined complete-standard with an AARE of 0.0757 and complete models with an AARE of 0.0765 for test data provide suerior predictions compared to other models checked. The ratio of $(K_b J_0)/(K_s)$ is calculated to be 2.32 for complete-standard model showing that the complete model is the dominant mechanism and more pore blockage occurs

in the filtration [18]. According to complete model mechanism the particles with size smaller than filter media pores, penetrate in pores and adhere to the inner wall. Accumulation of such particles eventually led to pore blocking and rapid filtrate flux reduction.

Operation of the two separation processes of filtration alone and centrifuge-filtration can be compared for turbidity removal and filtrate flux under 4 bars of pressure difference across filter media. The results show that the cumulative flux achievable infiltration of fermented solution is 2.174 L/m^2 h after 350 minutes of operation. Such low cumulative flux is due to formation and compression of cake layer on ceramic filter. Filtration of centrifuged solution provide a cumulative flux of 31.494 L/m^2 h after 50 minutes of operation. Obviously, from the filtrate flux point of view centrifuge-filtration seems to be superior to filtration of fermented solution. The measured turbidity removal under 4 bars pressure difference across filter media is 96.99% for the filtration of fermented solution which is higher than 89.78% for the filtration of centrifuged solution. This is due to the cake layer formed during the filtration of fermented solution that allows the removal of most of the suspended solids in the solution. It is worth noting that the difference in cumulative flux between the two processes is of one order of magnitude. Thus, one can conclude that in spite of higher product turbidity in the centrifuge-filtration process, it works much better than the filtration of fermented solution.

CONCLUSIONS

Filtration process is examined for removal of suspended solids from fermented solution of sugarcane molasses. To evaluate the filtration performance of the fermented solution by ceramic filter, four operating pressures are tested. For a given operating time, as the pressure increases to 4 bars, flux is decreased and turbidity removal is increased to 96.99%. Based on the ANOVA analysis of the blocking models predictions, the cake-complete model can best fit experimental data with an AARE of 0.112. Separation of suspended solids by centrifugal separator is also investigated by full factorial experimental design using time and centrifuge speed as the independent variables. Correlative models that are developed for predicting energy consumption and product solution turbidity showed relative errors of less-equal 6% in validation tests. The correlative models can be used to optimize operating conditions. Centrifugation under optimal operation conditions of 3 minutes and 1920 rpm leads to 80% turbidity removal, which corresponds to the removal of particles with sizes greater than 4.5 (μm) in fermented solution. Validation tests for predicting optimal turbidity and energy consumption showed relative errors of 7% and 2%, respectively. The pores blocking and flux reduction in the filtration after centrifugation is best described by a complete model with AARE of 0.0841. The centrifuge-filtration process has much higher cumulative flux and lower turbidity removal compared to filtration alone which makes it a more desirable choice in many industrial applications.

Nomenclatures

Volume filtered through available membrane area (m^3/m^2)	V
Initial flux (m/s)	J_0
Complete blocking constant (1/s)	K_b
Standard blocking constant (1/m)	K_s
Intermediate blocking constant (1/m)	K_i
Cake filtration constant (s/m^2)	K_c
Time of filtration (s)	t
Centrifugation time (min)	t_c
Speed of centrifuge (rpm)	ω
Experiment data	Y_{exp}
Model prediction	Y_m
Total number of data	n
Average Absolute Relative Error	AARE
Sum of Squared Residual	SSR

Received: Dec. 13, 2023; Accepted: May. 22, 2023

REFERENCES

[1] Gomes M.C.S., Moreira W.M., Paschoal S.M., Sipoli C.C., Suzuki R.M., Sgorlon J.G., Pereira N.C., Modeling of Fouling Mechanisms in the Biodiesel Purification Using Ceramic Membranes, *Separation and Purification Technology*, **269:** 118595 (2021).

[2] Dalena F., Senatore A., Tursi A., Basile A., "Bioenergy Production from Second- and Third-Generation Feedstocks", *Elsevier Ltd*, 559-599 (2017).

[3] Najafpour G., Younesi H., Ku Ismail K.S., Ethanol Fermentation in an Immobilized Cell Reactor Using Saccharomyces Cerevisiae, *Bioresour. Technol.*, **92(3):** 251-260 (2004).

[4] Santos F., Eichler P., de Queiroz J.H., Gomes F., "Production of Second-Generation Ethanol from Sugarcane", Elsevier Inc., 195-228 (2020).
[5] Cardona Alzate C.A., Sánchez Toro O.J., Energy Consumption Analysis of Integrated Flowsheets for Production of Fuel Ethanol from Lignocellulosic Biomass, *Energy*, **31(13):** 2447-2459 (2006).
[6] Bajpai P., "Advances in Bioethanol", Springer Briefs in Applied Sciences and Technology, 1-12 (2013).
[7] Baptista C.M.S.G., Cóias J.M.A., Oliveira A.C.M., Natural Immobilisation of Microorganisms for Continuous Ethanol Production, *Enzyme. Microb. Technol.*, **40(1):** 127-131 (2006).
[8] Göksungur Y., Zorlu N., Production of Ethanol from Beet Molasses by Ca-Alginate Immobilized Yeast Cells in a Packed-Bed Bioreactor, *Turkish J. Biol.*, **25(3):** 265-275 (2001).
[9] Sjölin M., Thuvander J., Wallberg O., Lipnizki F., Purification of Sucrose in Sugar Beet Molasses by Utilizing Ceramic Nanofiltration and Ultrafiltration Membranes, *Membranes*, **10(1):** 5 (2019).
[10] Saha K., Maharana A., Sikder J., Chakraborty S., Curcio S., Drioli E., Continuous Production of Bioethanol from Sugarcane Bagasse and Downstream Purification Using Membrane Integrated Bioreactor, *Catalysis Today*, **331:** 68-77 (2019).
[11] Chi Tien., "Principles of Filtration", Elsevier Science (2012).
[12] Grenier A., Meireles M., Aimar P., Carvin P., Analysing Flux Decline in Dead-End Filtration, *Chem. Eng. Res. Des.*, **86(11):** 1281-1293 (2008).
[13] Heidari S., Amirinejad M., Mirzadeh S.S., Wood D.A., Insights into Colloidal Membrane Fouling Mechanisms for Nanofiltration of Surface Water Using Single and Hybrid Membrane Processes, *Polymers for Advanced Technologies*, **32(6):** 2517-2530 (2021).
[14] Gonsalves V.E., A Critical Investigation on the Viscose Filtration Process, *Recueil des Travaux Chimiques des Pays-Bas*, **69(7):** 873-903 (1950).
[15] Grace H.P., Structure and Performance of Filter Media, *AIChE Journal*, **2(3):** 307-15 (1956).
[16] Shirato M., Aragaki T., Iritiani E ., Blocking Filtration Laws for Filtration Law Non-Newtonian Fluids, *Journal of Chemical Engineering of Japan*, **12(2):** 162-164 (1979).
[17] Jacques H., Mathematical Models and Design Methods in Solid-Liquid Separation, *NATO ASI Ser. Ser. E Appl. Sci.*, **88:** 83-89 (1985).
[18] Bolton G., Lacasse D., Kuriyel R., Combined Models of Membrane Fouling : Development and Application to Microfiltration and Ultrafiltration of Biological Fluids, *Journal of Membrane Science*, **277:** 75-84 (2006).
[19] Bowen W.R., Gan Q., Properties of Microfiltration Membranes: Flux Loss during Constant Pressure Permeation of Bovine Serum Albumin, *Biotechnol. Bioeng.*, **38(7):** 688-696 (1991).
[20] Mahesh Kumar S., Roy S., Filtration Characteristics in Dead-End Microfiltration of Living Saccharomyces Cerevisiae Cells by Alumina Membranes, *Desalination*, **229(1-3):** 348-361 (2008).
[21] Sampath M., Shukla A., Rathore A.S., Modeling of Filtration Processes—Microfiltration and Depth Filtration for Harvest of a Therapeutic Protein Expressed in Pichia Pastoris at Constant Pressure, *Bioengineering*, **1(4):** 260-277 (2014).
[22] Zhu Z., Mhemdi H., Dead end Ultra- Fi Ltration of Sugar Beet Juice Expressed from Cold Electrically Pre-Treated Slices : Effect of Membrane Polymer on Fouling Mechanism and Permeate Quality, *Innov Food Sci Emerg Technol*, **36:** 75-82 (2016).
[23] Kovaleva O.A., Lazarev S.I., Kovalev S.V., Effect of Transmembrane Pressure on Microfiltration Concentration of Yeast Biomass, *Petroleum Chemistry*, **57:** 974-982 (2017).
[24] Saleem M., Alibardi L., Cossu R., Cristina M., Spagni A., Analysis of Fouling Development under Dynamic Membrane Filtration Operation, *Chem. Eng. J.*, **312:** 136-143 (2017).
[25] Shi C., Rackemann D.W., Moghaddam L., Wei B., Li K., Lu H., Xie C., Hang F., Doherty W.O., Ceramic Membrane Filtration of Factory Sugarcane Juice: Effect of Pretreatment on Permeate Flux, Juice Quality and Fouling, *Jou. Food Eng.*, **243:** 101-113 (2019).
[26] Choobar B.G., Shahmirzadi M.A.A., Kargari A., Manouchehri M., Fouling Mechanism Identification and Analysis in Microfiltration of Laundry Wastewater., *Jou. Envir. Chem. Eng.*, **7(2):** 103030 (2019).
[27] Schippers J.C., Verdouw J., The Modified Fouling Index, a Method of Determining the Fouling Characteristics of Water, *Desalination*, **32:** 137-148 (1980).